International Journal of Microwave and Wireless Technologies

cambridge.org/mrf

Investigation of 10-port coupled fed slotted MIMO antenna system for 5G mobile handset

D. Rajesh Kumar, G. Venkat Babu, K.G. Sujanth Narayan and N. Raju

Centre of Excellence in RF System Engineering, SASTRA Deemed to be University, Thanjavur, Tamilnadu, India

Research Paper

Cite this article: Kumar DR, Babu GV, Narayan KGS, Raju N (2022). Investigation of 10-port coupled fed slotted MIMO antenna system for 5G mobile handset. *International Journal of Microwave and Wireless Technologies* **14**, 892–905. https://doi.org/10.1017/S1759078721001112

Received: 18 December 2020
Revised: 27 June 2021
Accepted: 30 June 2021
First published online: 22 July 2021

Key words:
5G; channel capacity; MIMO; SAR; WLAN

Author for correspondence:
G. Venkat Babu,
E-mail: venkatbabu@ece.sastra.edu

Abstract

A dual-band 10-port multiple input multiple output (MIMO) antenna array for 5G smartphone is proposed. Each antenna in the MIMO system can work from 3.4 to 3.6 GHz and 5 to 6 GHz with 10 dB (2:1 VSWR) impedance bandwidth. Nevertheless, for a 3:1 VSWR, the antenna operates from 3.3 to 3.8 GHz and 4.67 to 6.24 GHz. The MIMO system is formed by making 10 seven-shaped coupled fed slot antenna elements excited at two different resonant modes and integrated into the system circuit board. By implementing the spatial and polarization diversity techniques, high isolation better than 28 dB between any pair of antenna elements is achieved. The proposed 10-port MIMO antenna array is fabricated and measured. Significant radiation efficiency is obtained, ranging from 65 to 82% for both bands. The antenna gain in the required operating band is substantial, around 3–3.8 dBi. Further, the MIMO parameters such as envelope correlation co-efficient, channel capacity, and total active reflection co-efficient are calculated. The antenna's robustness is estimated by analyzing the user hand effects and specific absorption rate (SAR). The measured results are well agreed with the simulated results.

Introduction

Nowadays, smartphones are becoming more and more popular because of their versatile functions such as communications, Internet of Things (IoT), entertainment, financial services and navigation, etc. Therefore, improving the radio signal transmission performance in mobile phones is of paramount importance and has turned into a hotspot research area in the field of RF communication. The multiple input multiple output (MIMO) technology has gained importance in improving the performance of the overall system as its advantage lies in providing increased data rate and high spectrum efficiency without compensating the transmitting power and bandwidth [1]. Therefore, it is a promising technology that can be used in future 5G communication [2]. For 5 G mobile handsets, a compact, multi/wideband antenna system with high isolation and efficiency is needed [3]. In the recent past, various MIMO antenna systems have been proposed for 5G smartphones targeting the sub-6 GHz spectrum [4–14]. The smartphone antennas presented in the above works provide a single-band operation with a narrow bandwidth (<200 MHz) by occupying the large space in the printed circuit board, which increases the system complexity during fabrication. The antenna in the 5G smartphones should be smaller in size to increase the number of antennas to exhibit better MIMO performance. But isolation becomes a serious issue when more antennas are on the system board, as it degrades the overall system performance (efficiency, envelope correlation co-efficient (ECC), channel capacity, etc.).

Few dual-band 5G MIMO antennas have been presented to cover the sub-6 GHz spectrum in recent years [15–19]. Among these reported antennas, most have reflection co-efficient <−6 dB and isolation better than 13 dB only. In [15], an eight-port MIMO antenna system covering 3.4–3.6 and 5.15–5.925 GHz is proposed. Though the lower band provides −10 dB bandwidth, the higher band covers only −6 dB impedance bandwidth. The 10-port multi-band (3.4–3.8 and 5.15–5.925 GHz) antenna reported in [16] is able to provide only −6 dB bandwidth with isolation better than 11 dB. A 5G antenna array composed of 10 identical monopole antennas covering the bands 3.31–3.96 and 4.3–5.18 GHz with −6 dB impedance bandwidth is presented [17]. But the MIMO antenna can provide isolation better than 12.7 dB only. In [18], a four-port MIMO antenna system targeting 5 G NR bands at 3.5, 12.5, and 17 GHz for IoT applications is proposed. With the help of a complementary modified split ring resonator on the ground plane, isolation of >21 dB is obtained. An eight-element dual-band MIMO antenna for 5G smartphones working at 3.3–4.2 and 4.8–5 GHz with isolation >10 dB is presented in [19]. A compact two/four-port MIMO antenna for Wi-Max and 5G applications (2.74–4.41 GHz) is proposed. Meander line configurations are incorporated between the antenna elements to enhance isolation above 19 dB [20]. The quasi-orthogonal radiations produced by the two antennas offer pattern and polarization diversity, resulting in excellent isolation of more than 12 dB [21]. In [22], a highly isolated (>21 dB) two-port button MIMO

CAMBRIDGE UNIVERSITY PRESS

antenna for wearable application is presented. The defective ground plane, together with the copper ring surrounding the four holes of the button, makes a significant contribution to high isolation between the antenna ports.

Space in mobile devices is strictly limited to the generic structure of the mobile phone design. Therefore, the components in the mobile system board are highly sensitive to isolation. Thus, while designing the MIMO antenna, care should be taken to enhance the isolation between the adjacent antenna elements to improve the system performance. Techniques such as neutralization line, defected ground structure, and orthogonal modes have been incorporated to enhance the isolation [23–37]. Furthermore, techniques have been listed in the reference [38–42], such as the asymmetrical arrangement of antenna elements, coupled fed inverted F antenna structures, self-isolated antenna designs, and antennas with conjoined sections have been discussed. In the above-reported literature, the isolation is enhanced by employing dedicated decoupling structures, which occupy additional space in the system board and add complexity during the fabrication. The easy and common technique carried out to enhance the isolation in MIMO antenna design is distance optimization [29, 43, 44]. An appropriate distance between the antenna elements is important when discussing the isolation, where no other decoupling structure is deployed. By optimizing the distance between the antenna elements, a high amount of isolation could be obtained.

In this paper, a dual-band 10-port antenna array for a 5G smartphone is proposed. Each antenna in the MIMO system can work from 3.4 to 3.6 GHz and 5 to 6 GHz with −10 dB impedance bandwidth. The MIMO system is formed by making 10 seven-shaped coupled fed slot antenna elements excited at two resonant modes of operation (3.4–3.6 and 5–6 GHz) and integrated into the system circuit board. The high isolation (>28 dB) between any antenna elements is achieved by implementing spatial and polarization diversity techniques. The proposed 10-port MIMO antenna array is fabricated and measured. The measured results are well agreed with the simulated results. Significant antenna efficiency is measured from 65 to 82% for both bands of operation. Further, the antenna parameters such as ECC, total active reflection co-efficient (TARC), and channel capacity are measured to analyze the performance of the MIMO system. The user hand effects and specific absorption ratio (SAR) are also studied.

The significance of this work can be summarized as follows:

- To the best of the author's knowledge, this is the first MIMO antenna of its kind to have measured isolation between any adjacent pair is better than 28 dB without employing any decoupling mechanism.
- Due to such enhancement in isolation, MIMO parameters such as ECC (<0.035) and TARC (>10 dB) are better than acceptable ranges for a MIMO antenna system for 5G mobile phones. According to [45], antenna parameters such as isolation and ECCs have a significant impact on the efficiency and diverse performance of a MIMO device. The higher the antenna isolation, the smaller the ECC, resulting in greater diversity and channel capacities. Improving isolation also increases channel bandwidth, resulting in more efficient spectrum utilization.
- Moreover, from the literature, it is observed that dual-band MIMO antenna systems for 5G smartphones targeting the spectrum (3.4–3.6 and 5–6 GHz) provide only −6 dB impedance bandwidth in either of the bands. But the MIMO antenna proposed in this work covers both the spectrum in −10 dB bandwidth (2:1 VSWR).

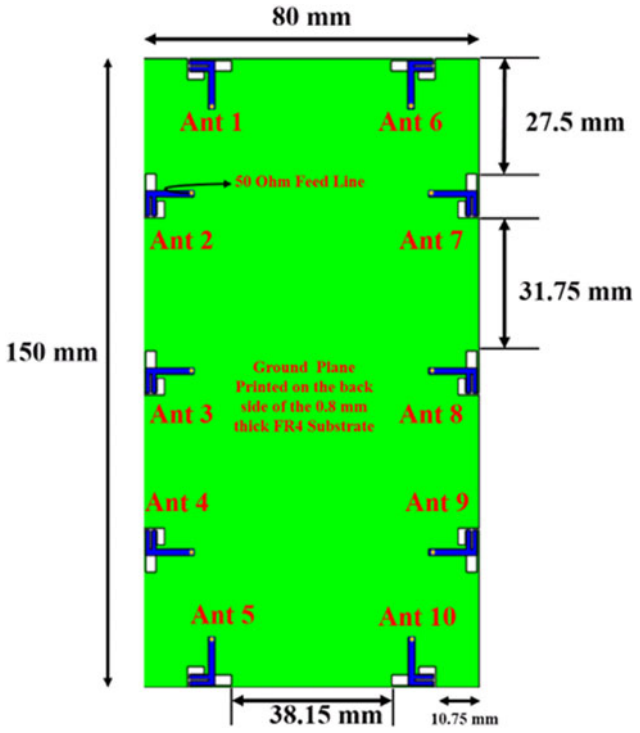

Fig. 1. Overall structure and dimension of the proposed antenna.

MIMO antenna design and analysis

The geometry of the proposed 10-port MIMO antenna is illustrated in Fig. 1. All the antenna elements are printed on the four side edges (top, bottom, left, and right) of the FR4 substrate (relative permittivity 4.6 and loss tangent 0.02) of dimension $180 \times 40 \times 0.8\ mm^3$, which is compatible with 5.7-inch smartphones. Antenna elements 1–5 are disposed of on the left, and the rest are printed on the substrate's right-side edges. The structure and dimension of an individual element (Antenna 1) are shown in Fig. 2. In the proposed design, each antenna can cover the two LTE bands ranging from 3.4 to 3.6 and 5 to 6 GHz, respectively. Initially, two rectangular-shaped slots of size 10.5×2.5 and $4 \times 1.8\ mm^2$ are etched on the ground plane, and they are connected by a tiny rectangular slot of $0.5 \times 0.2\ mm^2$. A square slot of size $0.5 \times 0.5\ mm^2$ is etched at the top edge of the ground plane to form the seven-shaped slots. Each radiating slot is fed by a 50 Ω F-shaped feeding strip printed on the other side of the substrate. The feeding strip is made up of three parts: a vertical part (50 Ω feed line) of size $11.5 \times 1.5\ mm^2$ and two horizontal stubs ($6 \times 1\ mm^2$) separated by 0.5 mm. All the dimensions described in this work are finalized after performing the parametric study using Keysight's Electro-Magnetic Professional (EMPro) commercial software.

The simulated *S*-parameters such as reflection coefficients and transmission coefficients of the proposed 10 antenna array are shown in Figs 3(a) and 3(b). As the proposed antenna is vertically symmetric, the results of antenna elements 1–5 are alone depicted. As shown in Fig. 3(a), all the antenna elements are

https://doi.org/10.1017/S1759078721001112 Published online by Cambridge University Press

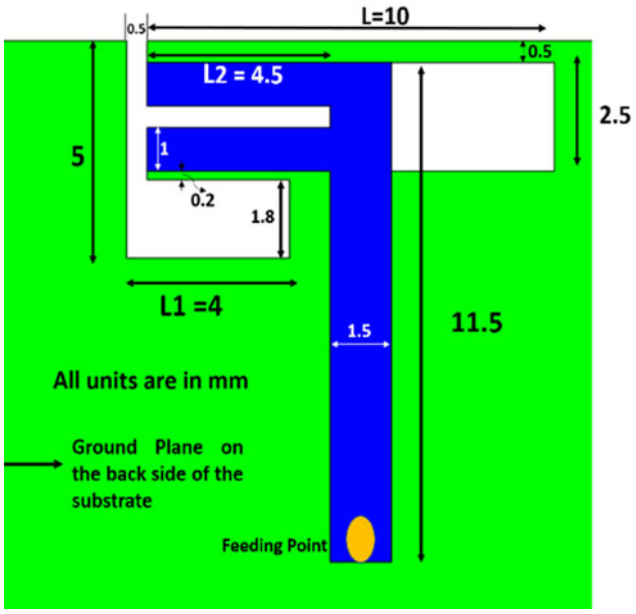

Fig. 2. Detailed dimension of the Antenna 1.

excited by two resonant modes, approximately at 3.4–3.6 and 5–6 GHz with −10 dB bandwidth. Figure 3(b) shows the transmission co-efficient across the two bands, and they are better than 28 dB between any pair of adjacent elements. The results are significantly adequate for the 5G MIMO antenna design. It is noteworthy that, though the separation between the antenna elements 1 & 2 and 3 & 4 is small, the isolation is still better than 28 dB.

The operation of seven-shaped antenna is described with the help of surface current distribution when antenna 1 is excited at 3.5 and 5.5 GHz, as shown in Figs 4(a)–4(d). One can see that, when antenna 1 is excited at both 3.5 and 5.5 GHz, its corresponding surface current on the ground plane does not spread toward its adjacent antenna port, demonstrating that the coupling effect is very weak, as shown in Figs 4(a) and 4(b).

Moreover, it is observed that the surface current density around the antenna is relatively localized. Outside the excited antenna, the magnitude of the current drops rapidly, which reduces the electromagnetic interference with adjacent radiating elements. When antenna 1 is excited for lower band (3.4–3.6 GHz), the current distribution around the closed end of the longer slot is maximum, as shown in Fig. 4(c), and for high band (5–6 GHz), the closed end of the shorter slot is maximum as shown in Fig. 4(d). For both resonating modes, the current at the open end is zero because, for an open slot antenna, the impedance will be maximum at the opening section and minimum at the closed end.

This infers that the electric field at both 3.5 and 5.5 GHz is maximum at the two open ends of the seven-shaped slots, as shown in Figs 5(a) and 5(b). It proves that one-quarter wavelength mode ($\lambda/4$) is the fundamental mode for the open end of the seven-shaped slots.

The simulated vector electric field distributions along the ground plane, when antenna 1 and 6 are excited, are shown in Figs 6(a)–6(d). When antennas 1 and 6 are excited separately (at 3.5 and 5.5 GHz), the coupling electric field between antennas 1 & 2 and 6 & 7 is weak (the null field is observed), as illustrated

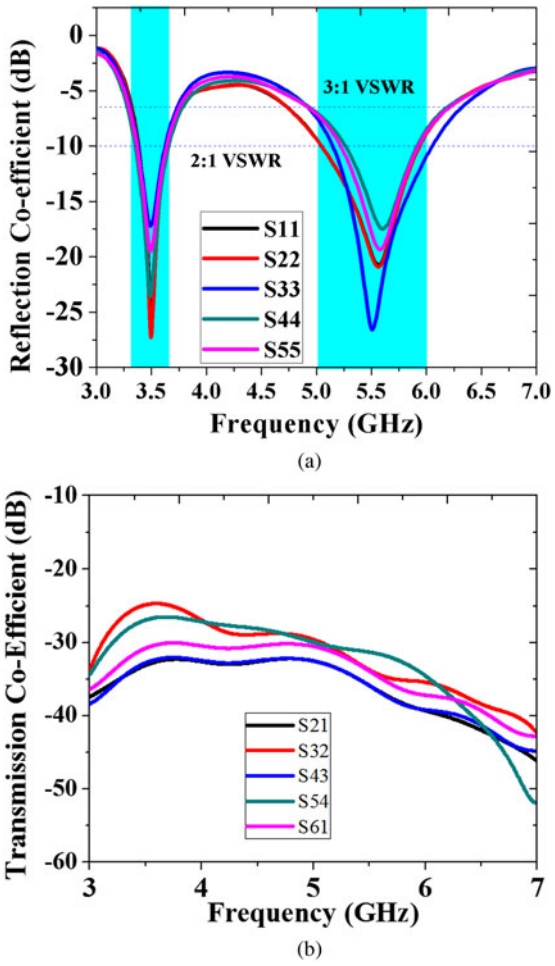

Fig. 3. Simulated (a) reflection co-efficient, simulated (b) transmission co-efficient.

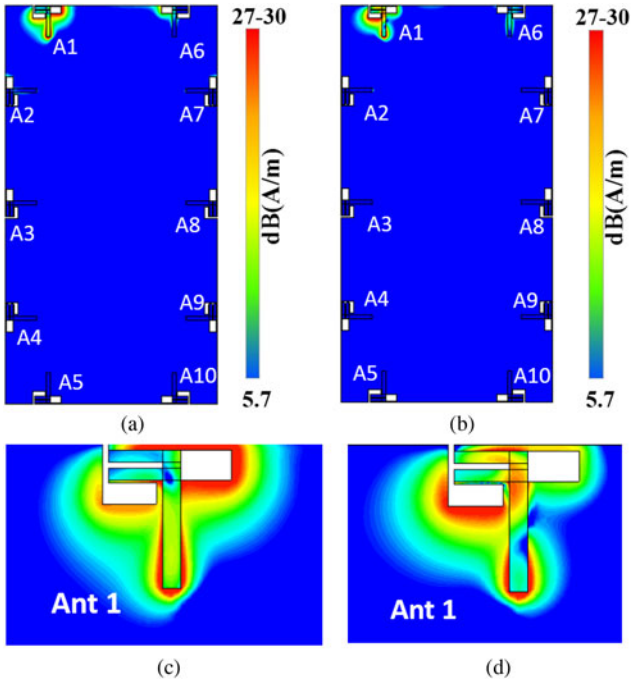

Fig. 4. Simulated overall surface current distribution, when Ant 1 is excited at (a) 3.5 GHz, (b) 5.5 GHz, enlarged view of Ant 1 when excited at (c) 3.5 GHz, (d) 5.5 GHz.

https://doi.org/10.1017/S1759078721001112 Published online by Cambridge University Press

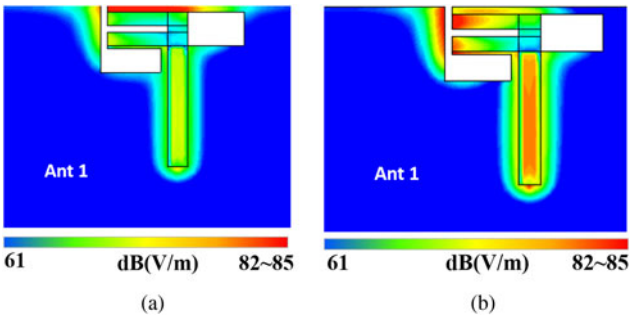

Fig. 5. Simulated electric field distribution when Ant 1 is excited at (a) 3.5 GHz, (b) 5.5 GHz.

in Figs 6(a)–6(d). It is because antennas 1 & 2 and 6 & 7 are disposed orthogonal to each other and exhibit orthogonal polarization (or polarization diversity).

The polarization diversity is explained with the help of a simulated three-dimensional radiation pattern, as shown in Figs 7(a)–7(d). As shown in Figs 7(a) and 7(c), the maximum radiation takes place in $+y$ direction for both the bands, when antenna 1 (horizontal antenna) is excited. On the other hand, when antenna 2 (vertical antenna) is excited for both the bands, the intense radiation is along the $-x$ direction as depicted in Figs 7(b) and 7(d). Thus, the polarization diversity is achieved by disposing the antennas orthogonal to each other, thereby enhancing the isolation.

The vector current distributions of antenna 1 at 3.5 and 5.5 GHz are shown in Figs 8(a) and 8(b). It is observed that the maximum current flows along the edges of the slot antenna toward the $+x$ direction for both the bands and it does not influence its adjacent antennas (2 and 6). Hence, it is quite apparent why the simulated isolation between the adjacent elements is better than 28 dB.

Parametric study

Some parametric studies have been illustrated in Figs 9(a)–9(c) to provide design guidelines for the proposed MIMO antenna array. When the lengths of the two slots (L and $L1$) are increased, the frequency of resonance for both the bands is shifted toward the lower frequency and *vice-versa*. Slot radiator lengths L and $L1$ are completely controlling two frequency bands. As shown in Figs 9(a) and 9(b), the impacts of varying slot lengths are analyzed. When tuning one length parameter, another parameter is kept constant. The results suggest that an increase in the lengths L and $L1$ will allow the low-band and high-band resonances to shift to the lower frequency and *vice-versa*. This is reasonable, as the low and high resonant modes are controlled by the longer and shorter open slots, respectively. The low and high-frequency bands are changed according to the lengths L and $L1$, respectively. Moreover, altering the length of $L1$ will not affect the lower band. Similarly, changes in the length L do not produce any effect on the high-frequency band. This result demonstrates that the frequency ratio of the two bands can be tuned (by changing L and $L1$) according to the desired operating frequencies. The variations in the length of the feeding strip ($L2$) mainly affect the impedance matching as well as shifting in the resonance of both the bands, as shown in Fig. 9(c).

Measured results and discussions

The proposed 10-port MIMO antenna array prototype is fabricated, as shown in Fig. 10, and tested. To carry out the

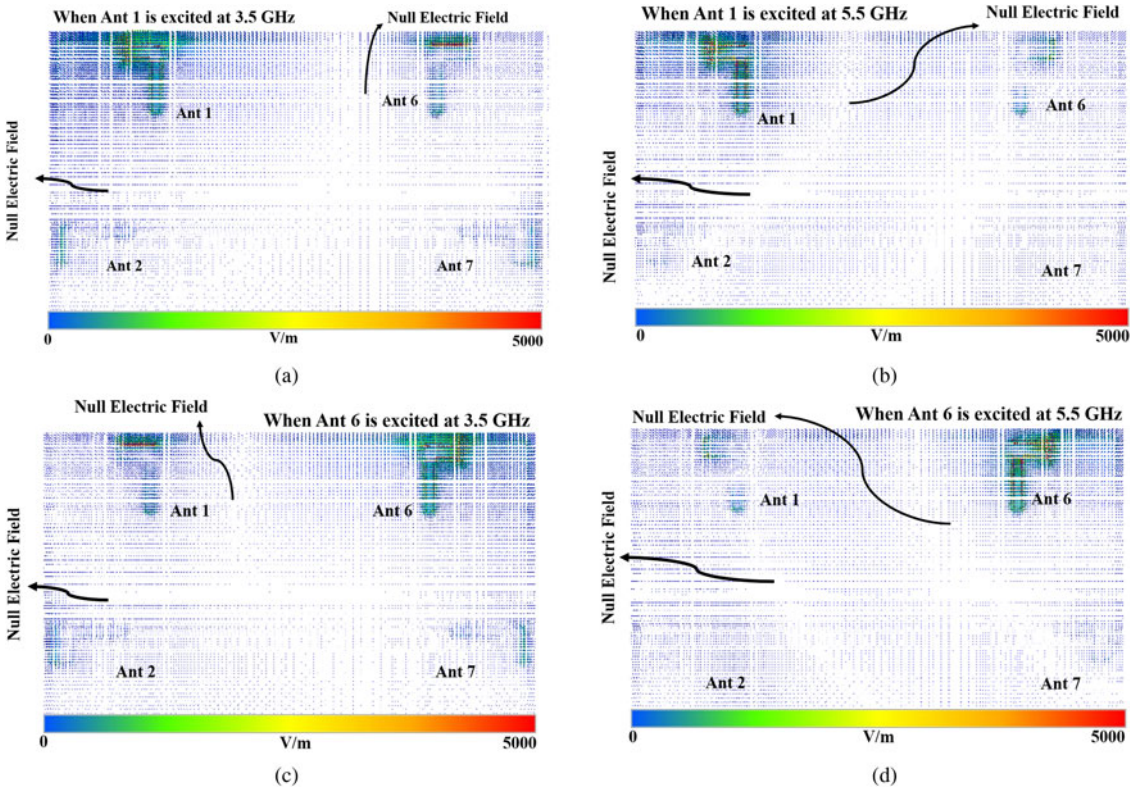

Fig. 6. Simulated vector electric field distributions when Ant 1 is excited at (a) 3.5 GHz, (b) 5.5 GHz, when Ant 6 is excited at (c) 3.5 GHz, (d) 5.5 GHz.

https://doi.org/10.1017/S1759078721001112 Published online by Cambridge University Press

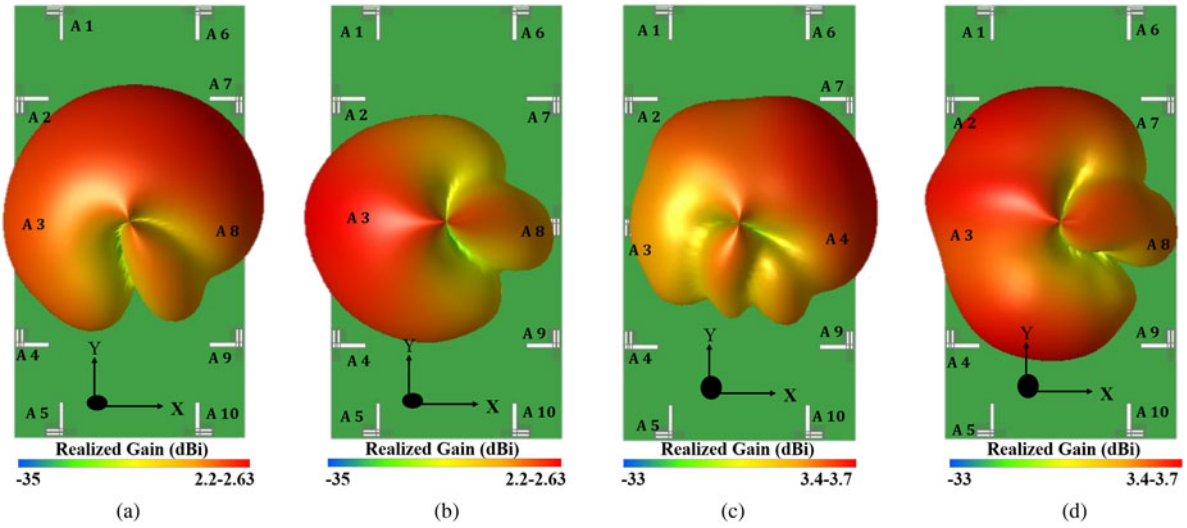

Fig. 7. Simulated three-dimensional radiation pattern when Ant 1 is excited at (a) 3.5 GHz, (b) 5.5 GHz, when Ant 2 is excited at (c) 3.5 GHz, (d) 5.5 GHz.

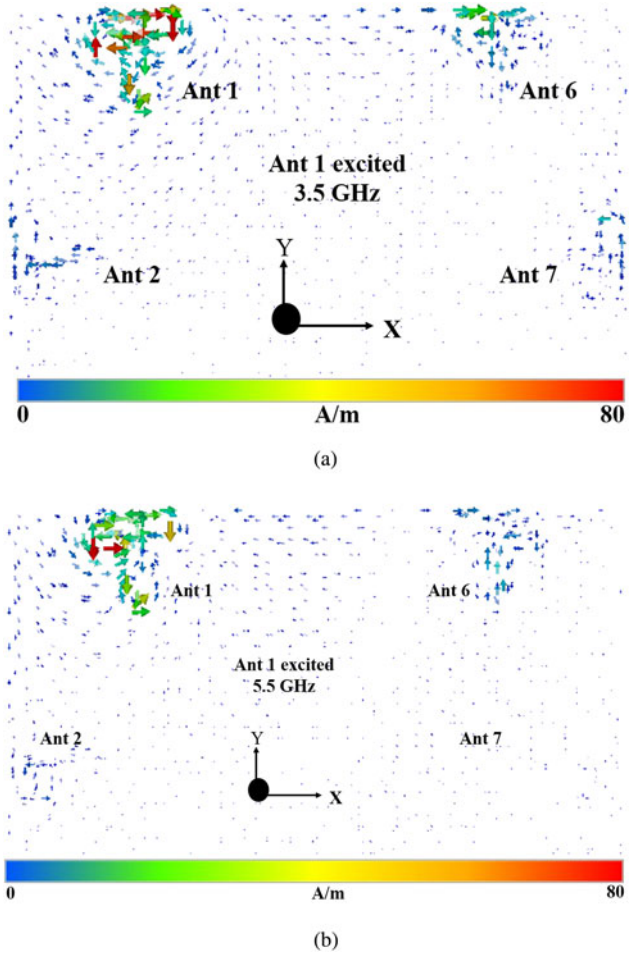

Fig. 8. Simulated vector current distribution when Ant 1 is excited at (a) 3.5 GHz, (b) 5.5 GHz.

measurements, 50 Ω Sub-Miniature-Version A (SMA) female connectors are soldered at the feeding strips of the antenna elements. The antenna parameters such as *S*-parameters, isolation, and radiation pattern are measured by terminating all antenna elements to 50 Ω matched loads when the antenna under the test is excited.

The measured reflection coefficient and isolation levels of the proposed antenna are shown in Figs 11(a)–11(c). The *S*-parameters are measured using Keysight's Firefox Network Analyzer N9917A. As shown in Fig. 11(b), the reflection coefficient of the antenna elements 1 to 5 well agreed with the simulated results. Each antenna has an impedance bandwidth (2:1 VSWR) of 200 MHz and 1 GHz at 3.5 and 5.5 GHz, respectively. Similarly, the isolation levels (Ant 1 to Ant 5) of adjacent antenna elements are shown in Fig. 11(c). For brevity, the isolation of other antennas has not been shown here. It is observed that all the antenna's isolation levels are better than 28 dB and well correlated with the simulated results.

To specify the coupling effects and diversity performance of the MIMO antenna systems, it is necessary to compute the MIMO parameters such as ECC and TARC from the measured far-field radiation pattern and *S*-parameters, respectively. The ECC and TARC for the proposed antenna are calculated from equations (1) and (3).

The ECC is an important parameter of a MIMO antenna system that can quantify the system's performance. The ECC of any two antennas can be calculated from the measured radiation pattern using equations (1) and (2) [31].

$$\mathrm{ECC} = \left| \frac{\oint\oint A_{ij}(\theta, \varphi) \sin\theta \, d\theta \, d\varphi}{\oint\oint A_{ii}(\theta, \varphi) \sin\theta \, d\theta \, d\varphi \, . \oint\oint A_{jj}(\theta, \varphi) \sin\theta d\theta d\varphi} \right|^2, \quad (1)$$

where

$$A_{ij} = E_{\theta,i}(\theta, \varphi) \, . \, E^*_{\theta,j}(\theta, \varphi) + E_{\varphi,i}(\theta, \varphi) \, . \, E^*_{\varphi,j}(\theta, \varphi). \quad (2)$$

As shown in Fig. 12(a), the measured ECCs of all the antenna pairs are <0.035, which is lower than the acceptable criterion of ECC <0.5. Low values of ECC will result in a higher diversity gain, which shows that the proposed 10-port antenna array possesses better diversity capability.

https://doi.org/10.1017/S1759078721001112 Published online by Cambridge University Press

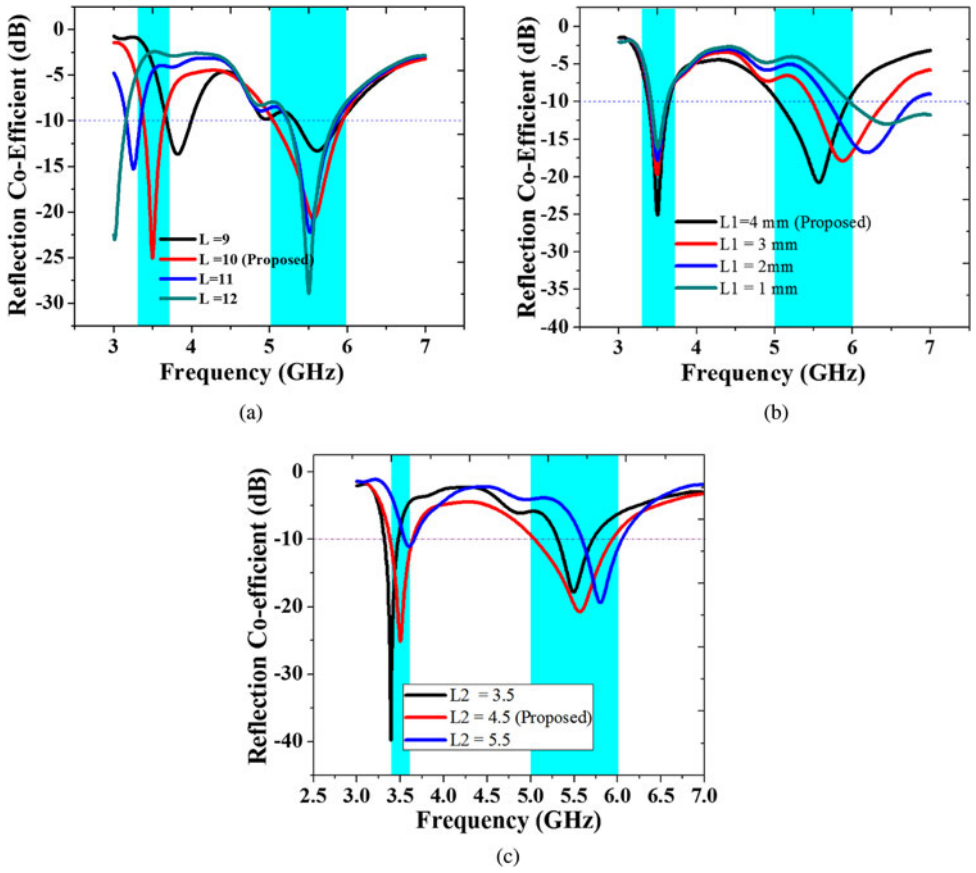

Fig. 9. Simulated reflection co-efficient of Ant1 for various values of (a) *L*, (b) *L*1, (c) *L*2.

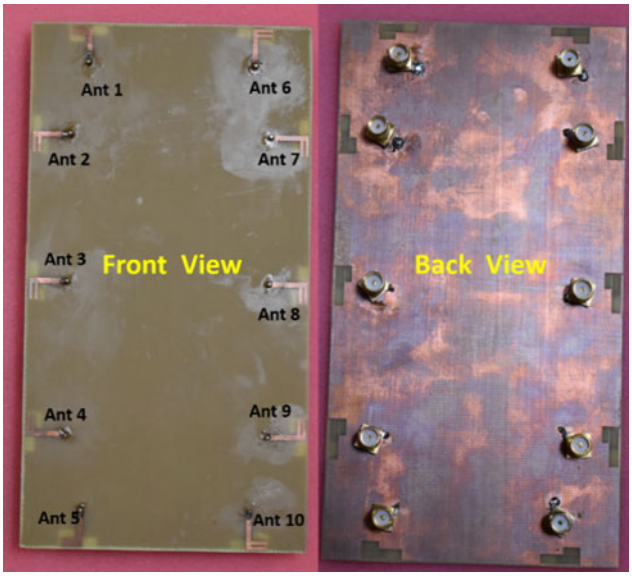

Fig. 10. Images of fabricated proposed MIMO antenna.

To further validate the performance and effective bandwidth of the MIMO antenna array, TARC are computed from the measured *S*-parameters using equation (3).

$$\text{TARC}\ (\Gamma) = \frac{\sqrt{|(S_{11} + S_{12}e^{j\theta})|^2 + |(S_{21} + S_{22}e^{j\theta})|^2}}{\sqrt{2}}. \quad (3)$$

The TARC curve is plotted for different excitation phases of other ports (with the same amplitude) with respect to port 1 as shown in Fig. 12(b). The proposed MIMO antenna is able to cover the desired frequency spectrum with −10 dB bandwidth while changing the excitation phases. This proves that the proposed design is highly suitable for 5G MIMO smartphone applications.

Figures 13(a)–13(d) show the measured radiation patterns of antenna elements 1 and 2 in the *xy* plane at 3.5 and 5.5 GHz, respectively. The patterns of other antenna components are not shown since the proposed antenna has a symmetrical arrangement. Both antennas have an omnidirectional radiation pattern over the operating bandwidth, as seen in Figs 13(a)–13(d). The maximum radiation (E-phi) for antenna 1 (horizontal antenna) resides at 90° and 30° at 3.5 and 5.5 GHz, respectively, as seen in Figs 13(a) and 13(b). In contrast, antenna 2 (vertical antenna), as seen in Figs 13(c)–13(d), exhibits maximum radiation at 180° and 240° for low band and high band, respectively. The maximum radiation of both horizontal antennas (Ant 1, 5, 6, and 10) and vertical antennas (Ant 2, 3, 4, 7, 8, and 9) is clearly complementary, demonstrating a significant pattern diversity feature.

Figure 14(a) shows the measured individual radiation efficiency of each element. The antenna efficiency is 63–80% for the low band (3.4–3.6 GHz) and 80–85% for the high band (5–6 GHz). Despite the small distance between the horizontal and vertical antennas (high coupling loss), the efficiency is >63%, ensuring that the proposed antenna has minimum channel capacity loss. The gain of the proposed 10-port MIMO antenna

https://doi.org/10.1017/S1759078721001112 Published online by Cambridge University Press

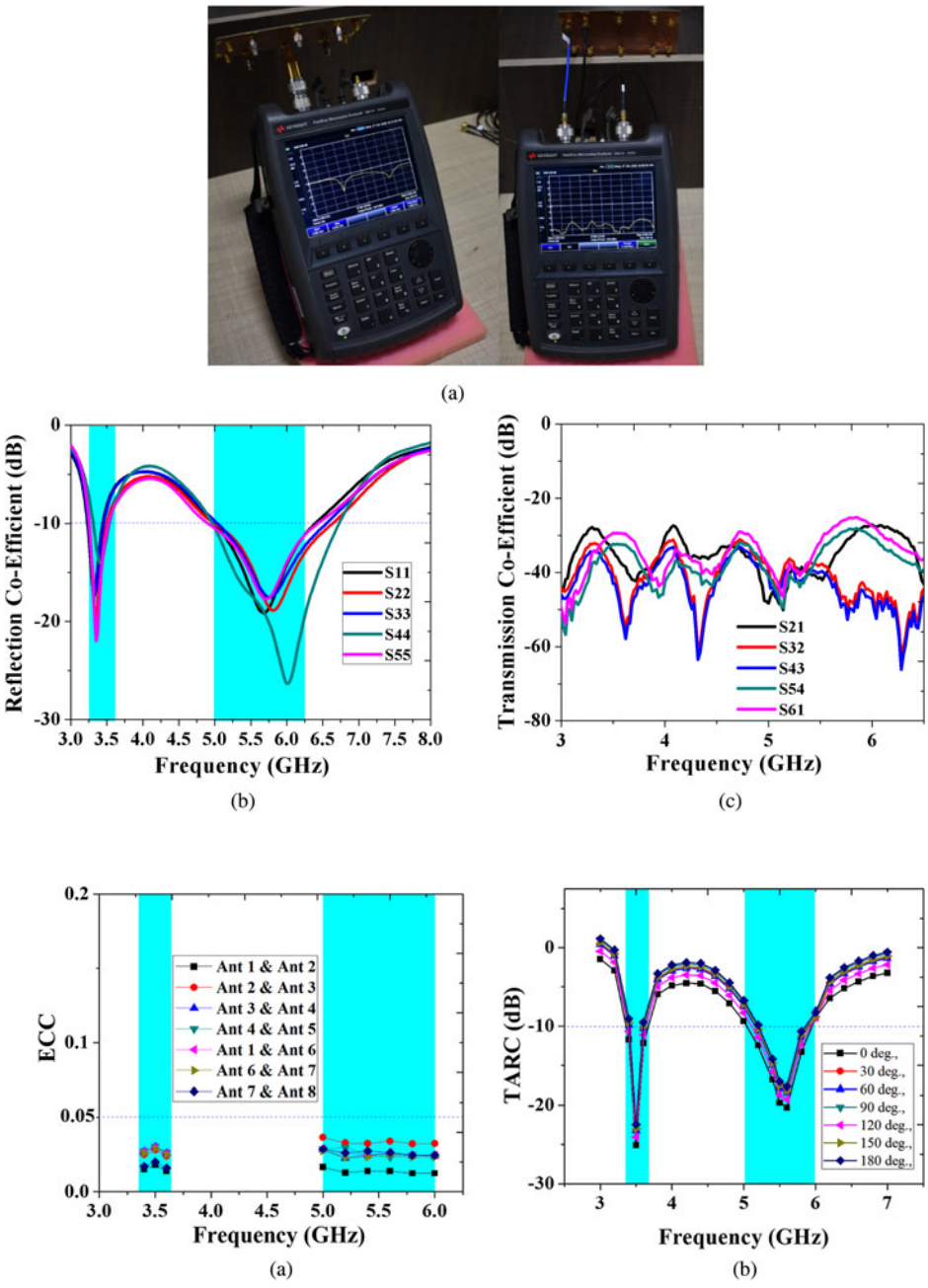

Fig. 11. (a) Measurement setup for *S*-parameters, (b) measured reflection co-efficient from Antenna 1 to 5, (c) measured transmission co-efficient.

Fig. 12. Measured (a) ECC, (b) TARC.

array, as seen in Fig. 14(b), varies from 3 to 3.8 dBi over the desired operating bandwidth, which is substantially higher for mobile phone applications.

MIMO performance

Channel capacity

From the radiation efficiency of the antenna element, the maximum channel capacity of the proposed 10-port antenna array is computed using equation (4), and it is about 46–48.5 bps/Hz for the low band and 51.7 bps/Hz for the high band at 20 dB SNR.

$$C = E\left(\log_2\left[\det\left(I + \frac{\mathrm{SNR}}{\eta_T} HH^T\right]\right)\right), \quad (4)$$

where I is the identity matrix, SNR is the average signal to noise ratio for the mobile terminal, η_T is the number of transmitting antennas, H is the Hermitian matrix, and H^T is the Hermitian transpose. The maximum ergodic channel capacities for an ideal MIMO system (antenna elements uncorrelated with each other and provide 100% efficiency) are 57.5 and 11.5 bps/Hz for 10×10 and 2×2 MIMO systems, respectively. Thus, the proposed 10-port MIMO antenna system provides a channel capacity 4.2 times higher than the ideal 2×2 MIMO system as shown in Fig. 15.

User hand effects

It is well understood that the antenna's performance will be affected when it is in proximity to the human hand. Hence,

https://doi.org/10.1017/S1759078721001112 Published online by Cambridge University Press

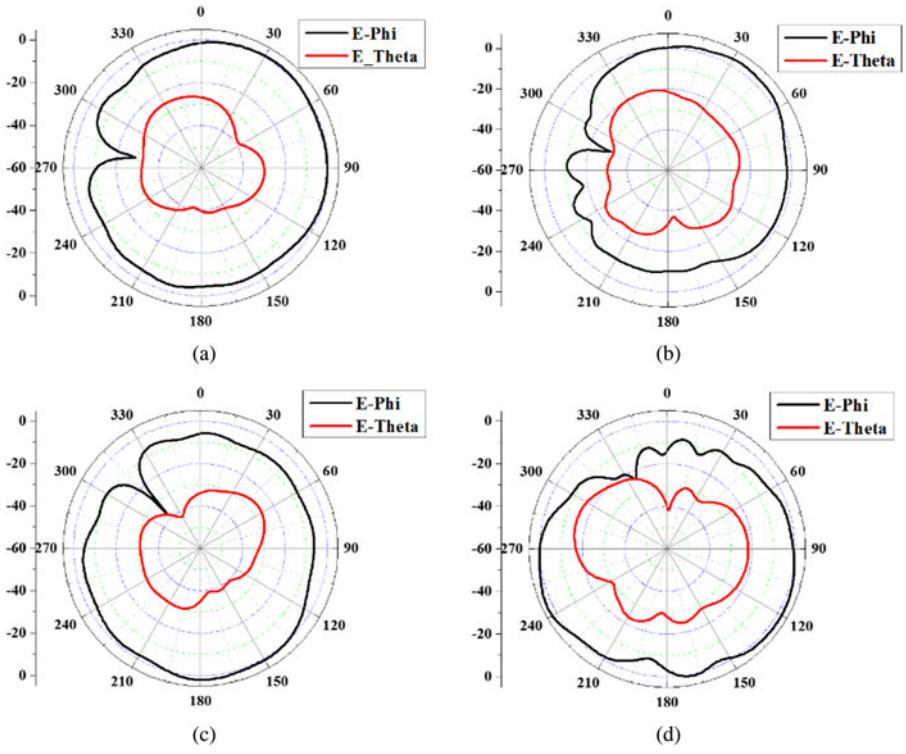

Fig. 13. Measured 2D radiation pattern of antenna 1 at (a) 3.5 GHz, (b) 5.5 GHz, antenna 2 at (c) 3.5 GHz, (d) 5.5 GHz.

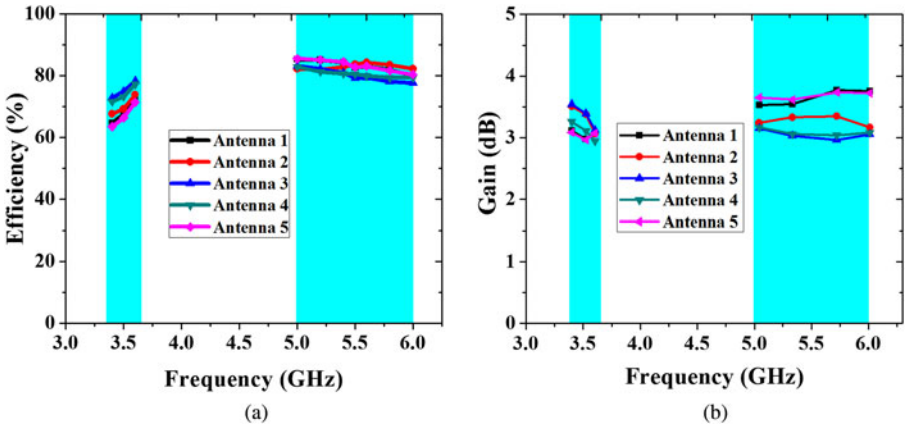

Fig. 14. (a) efficiency and (b) gain.

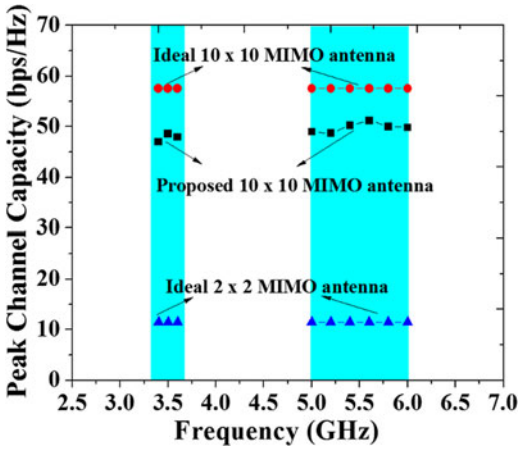

Fig. 15. Calculated peak channel capacity of the proposed antenna.

users' hand effects are investigated by including hand phantom in the simulation. There are two modes of hand operation used here to evaluate the performance; namely, single hand operation (SHO) and two hand operation (THO), as shown in Figs 16(a) and 16(b). Figures 17(a)–17(c) show the simulated *S*-parameters and the efficiency of the SHO. As antennas 2 and 3 are closer to the index and middle fingers, their reflection co-efficients are completely out of the band. Meanwhile, as the thumb finger is kept on antenna 7, its resonant frequency at the low band is shifted toward the right, as shown in Fig. 17(a). But the performance of all other antennas is almost unchanged in both the low and high bands. The isolation between the antenna elements during SHO is shown in Fig. 17(b). To have more accuracy, isolation between the adjacent antenna elements has been taken, and it is observed that isolation levels are better than 14 dB in both bands. The efficiency of the MIMO antenna during SHO is

https://doi.org/10.1017/S1759078721001112 Published online by Cambridge University Press

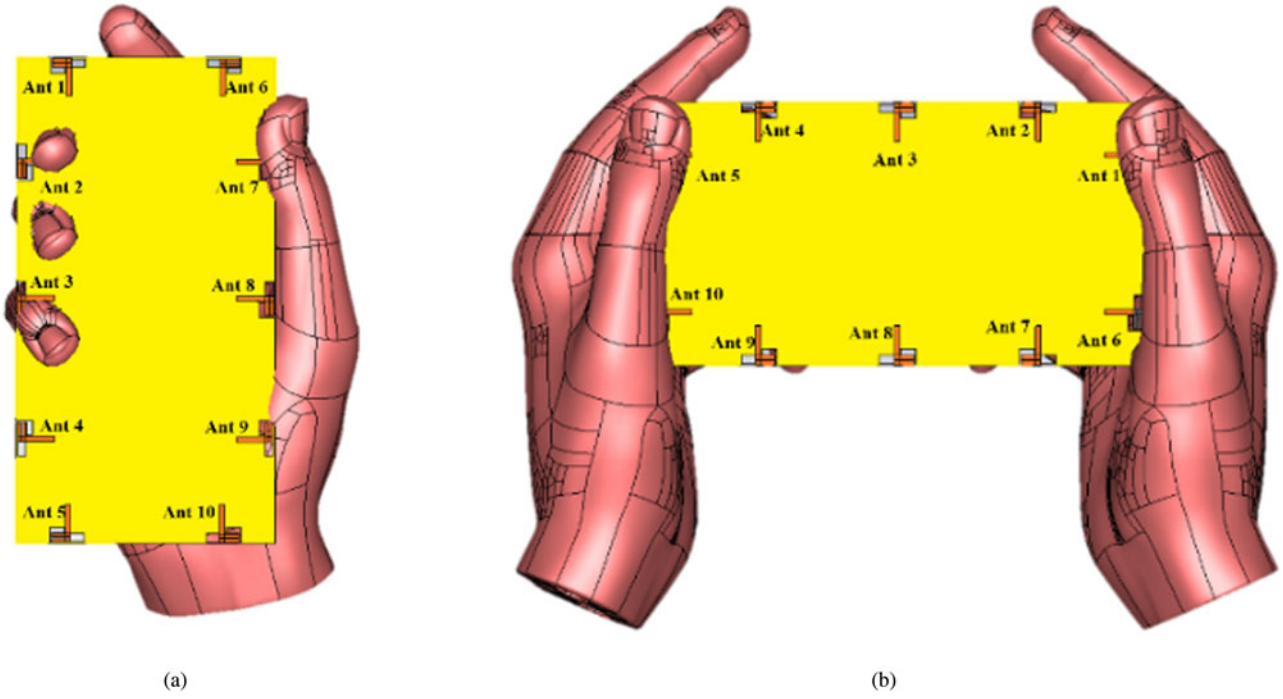

Fig. 16. (a) Single-hand operation (SHO), (b) two-hand operation (THO).

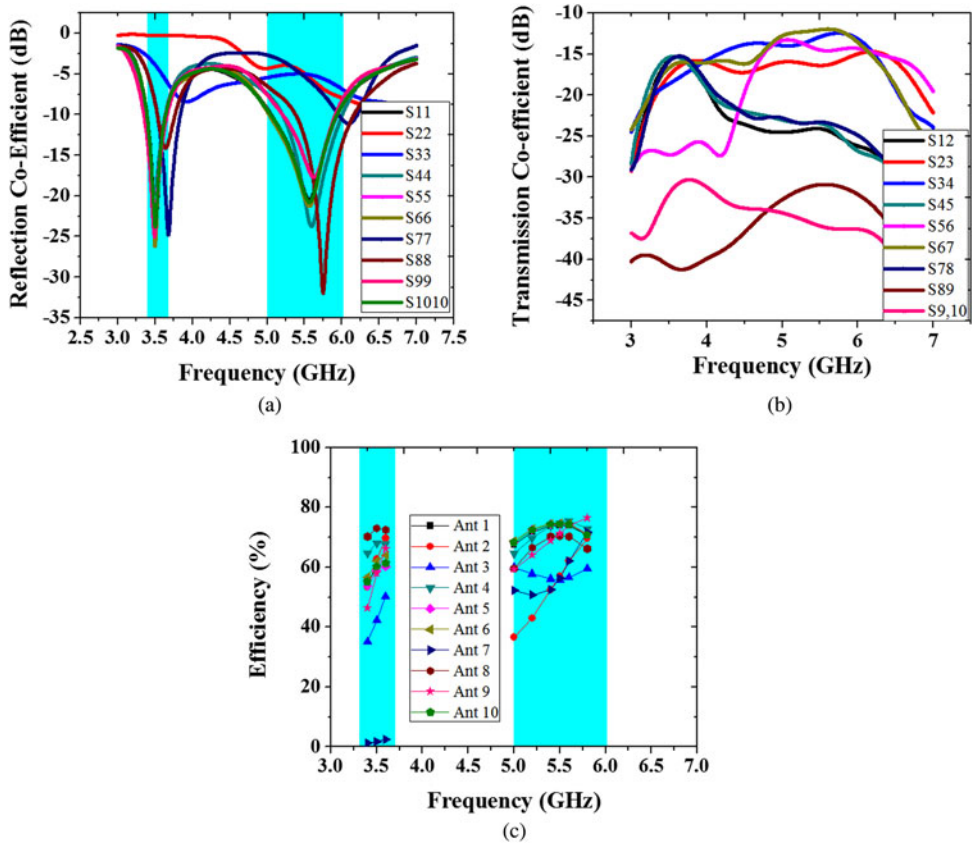

Fig. 17. Simulated performance of SHO, (a) reflection co-efficient, (b) transmission co-efficient, (c) efficiency.

shown in Fig. 17(c). Because antennas 2, 3, and 7 are so close to the user's hand, their efficiencies have been dropped below 50%. In particular, the efficiency of antenna 7 was drastically reduced below 10% in the low band. As for the remaining antennas, their radiation efficiencies are reduced and varied from 50 to 75% because they are still closer to the human hand phantom.

https://doi.org/10.1017/S1759078721001112 Published online by Cambridge University Press

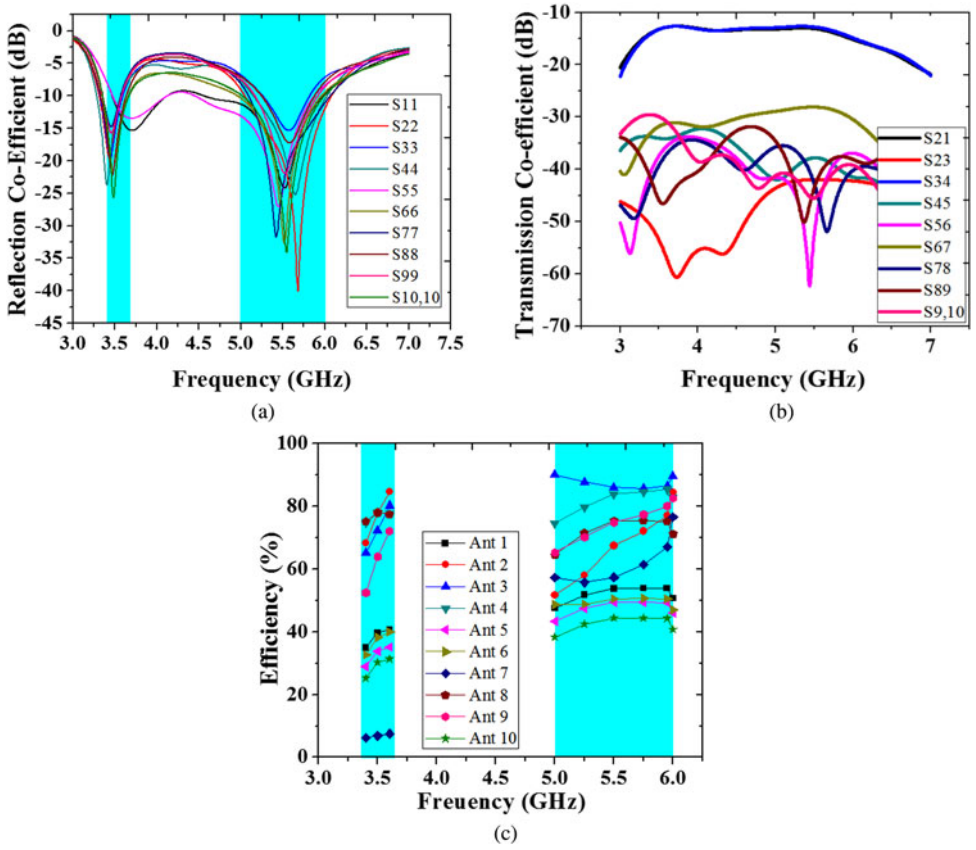

Fig. 18. Simulated performance of THO, (a) reflection co-efficient, (b) transmission co-efficient, (c) efficiency.

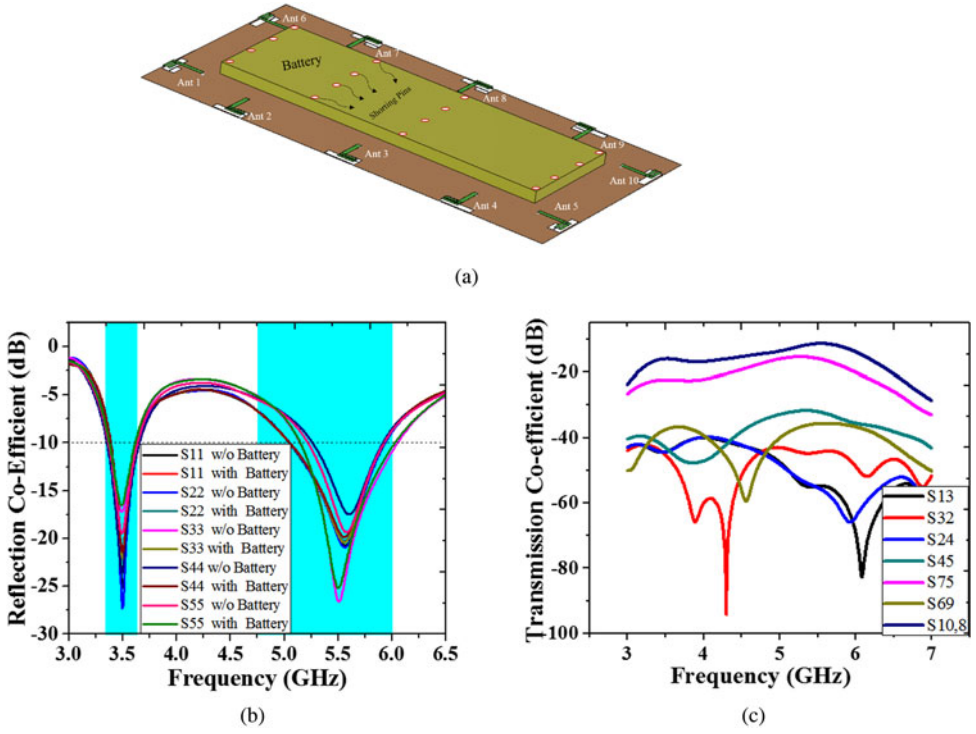

Fig. 19. Simulated (a) model of proposed antenna with battery, (b) reflection co-efficient with and without battery, (c) transmission co-efficient with battery.

https://doi.org/10.1017/S1759078721001112 Published online by Cambridge University Press

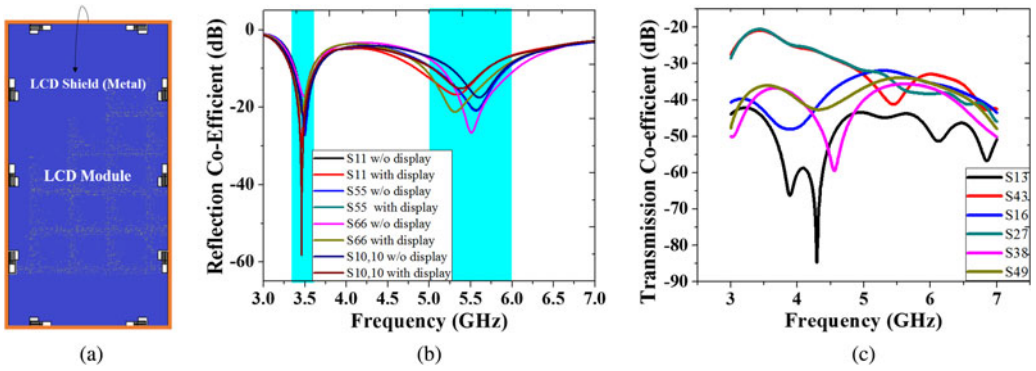

Fig. 20. Simulated (a) proposed antenna with LCD panel, (b) reflection co-efficient, (c) transmission co-efficient.

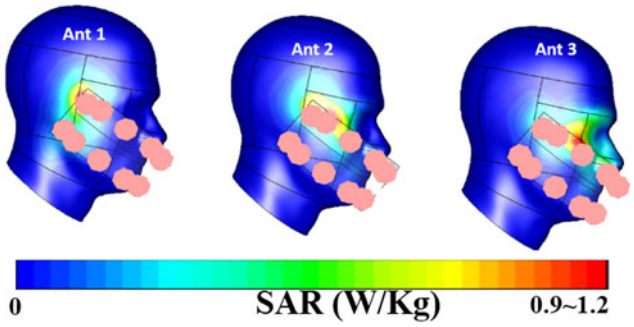

Fig. 21. SAR analysis of Ant 1–3 at 1(W/kg).

Likewise, the simulated reflection co-efficient, isolation, and the efficiencies of THO are shown in Figs 18(a)–18(c), respectively. Antennas 1, 5, 6, and 10 are in close proximity to the user's hand in this scenario. Hence, their reflection co-efficients are slightly shifted from the desired band (low band). Whereas the isolation between the adjacent elements is better than 14 dB. As shown in Fig. 18(c), efficiencies of antenna elements 1, 5, 6, and 10 are considerably reduced below 40%, and for the remaining antennas, the efficiencies are above 50%. The reason for the degradation mentioned above is that the human hands can absorb the radiating power from the antenna and attenuate it. On the whole, the proposed 10 antenna array is highly suitable for 5G mobile phone (3.4–3.6 and 5–6 GHz) applications.

Impacts of battery

Figure 19(a) shows the simulated model of the proposed antenna along with the battery. In this study, the rectangular metal block of size 118 mm × 40 mm × 4 mm is considered as a battery [44], and it is positioned on the front side of the substrate. The battery is electrically connected to the system ground plane via 16 shorting pins. As shown in Figs 19(b) and 19(c), the battery has a negligible influence on the antenna parameters such as reflection coefficient (>−10 dB) and the isolation (>18 dB).

Effects of LCD panel

The impact of panel display has also been investigated, as shown in Fig. 20(a). The LCD module comprises two parts: the LCD shield (metal) and the LCD panel. The LCD panel is modeled with the relative permittivity and loss tangent of 7 and 0.02, respectively [44]. The LCD module is disposed at a 2 mm distance from the ground plane. The LCD shield is connected to the ground plane; hence, it has proximity to the slot radiators. Due to this proximity to the radiators, there is a slight variation in both the reflection co-efficients and the isolation. But still, the MIMO array is able to achieve the reflection co-efficient >−10 dB and isolation >20 dB as shown in Figs 20(b)–20(c). The results show the MIMO array can exhibit desirable performance in the real-time environment.

Specific absorption rate

SAR is a significant parameter to be taken into account while designing a mobile phone antenna, because it estimates the amount of electromagnetic power absorbed by the human body. The head phantom is modeled for the proposed antenna, and SAR of antenna 1, 2, and 3 are observed. From Fig. 21, one can see that the maximum values of SAR are within 1.2 W/kg at 1 g of tissue. The SAR of the mobile phone antenna will be varied with respect to the distance between the mobile phone and the human head. The distance has been altered from 5 to 10 mm, and corresponding SAR has been estimated for our design. It is observed that the closer the distance between the antenna and the head phantom, the higher the value of SAR and *vice versa*.

Table 1 shows the performance comparison of the proposed MIMO antenna array with some other MIMO antenna arrays reported for 5G mobile handsets. It is apparent that the proposed antenna has very good isolation >28 dB, ECC <0.035, TARC >10 dB along with good radiation and MIMO performance.

Effects of metal frame

The metal frame of height 7 mm is added along the four side edges of the proposed MIMO antenna, as shown in Fig. 22(a) and simulated. The metal frame is printed on the 0.8 mm-thick FR4 substrate. However, the antenna with a metal frame can resonate in the two bands (3.5 and 5.5 GHz) as shown in Fig. 22(b). The simulated reflection co-efficients are very low compared with the non-metal frame environment, and transmission co-efficients are better than 12.5 dB only. The reason for the above loss in antenna's performance is that, according to electromagnetic image theory, when an antenna is located parallel to a conductor (metal frame), the radiation properties are seriously harmed by the out-of-phase electric current [46]. Therefore, the proposed antenna is highly suitable for non-metal frame mobile phone applications.

https://doi.org/10.1017/S1759078721001112 Published online by Cambridge University Press

Table 1 Performance comparison of the proposed work with previously published works

Reference	Center frequency (GHz)	Antenna dimension (mm^3) (single antenna)	Bandwidth (GHz)	Impedance bandwidth (dB)	Isolation (dB)	ECC	Efficiency	MEMO order	Peak channel capacity (bps/Hz)
[5]	3.6	25 × 25 × 11.6	3.3–3.9	−6	>15	<0.01	75	8	–
[15]	3.5/5.5375	14.9 × 4.6 × 0.8	3.4–3.6 and 5.15–5.925	−10/−6	>12	<0.1 and 0.04	50–56 (LB), 53–65 (HB)	8	38.8 (LB) 39.7 (HB)
[16]	3.6/5.5375	16.2 × 3 × 0.8	3.4–3.8 and 5.15–5.925	−6	>10	<0.15 and 0.05	42–65 (LB) 62–82 (HB)	10	48 (LB) 51.4 (HB)
[17][a]	3.505 (LB) 4.93 (HB)	16 × 12.5 × 0.8	3.31–3.7 and 4.46–5.4	−6	>12.5	<0.45	42.5–79.5 (LB), 81.1–83.3 (HB)	10	–
[18][a]	3.5	18 × 14 × 3.2	3.4–3.6	−10	>21.73	<0.08	81	4	–
[19][a]	3.75 and 4.9	18.6 × 7 × 0.8	3.3–4.2 and 4.8–5	−6	>11.5 (LB) >15 (HB)	<0.1 (LB) <0.12 (HB)	53.8–76.5 (LB) 62.6–79.1 (HB)	8	39.5 (LB) 40 (HB)
[20]	3.5/5	15 × 3.1 × 7	3.4–3.6 and 4.8–5.1	−6	>11.5	<0.08 and 0.05	41–72 (LB), 40–85 (HB)	8	38.5 and 38
[21]	3.5	9.8 × 4.8 × 6 and 12.5 × 4.9 × 6	3.3–3.6	−6	>15	<0.15	60	8	35
[22]	2.55 and 3.45	6.8 × 6.6 × 4	2.4–2.7 and 3.3–3.6	−6	>12.5	<0.25	45–51	8	–
[28]	3.5	27.3 × 1.2 × 0.8 (slot antenna) 26.5 × 1 × 0.8 (loop antenna)	3.4–3.6	−6	>15	<0.16	45–73	8	–
[6]	3.5	12 × 12 × 1	3.3–3.6	−6	>10	<0.11	48.6–73.2	4	–
[29]	3.5	12 × 7 × 0.8	3.4–3.6	−6	>17	<0.07	49–61	8	–
[30]	3.5	28.4 × 1 × 0.8	3.4–3.6	−6	>16	<0.05	59–73	8	38.2–39.8
[33]	3.75	20 × 6 × 0.8	3.3–4.2	−6	>12	<0.1	52–78	8	–
[40]	3.5	40.8 × 3 × 0.8, 38.2 × 3.2 × 0.8	3.4–3.6	−6	>11.6	–	38.5–47.3	3	–
This work	3.5/5.5	10.5 × 5 × 0.8	3.4–3.6 and 5–6	−10	>28	<0.035	60–78 (LB), 70–85 (HB)	10	46–48.5 (LB), 51.7 (HB)

[a]Only 5G antennas are considered; LB, lower band; HB, higher band.

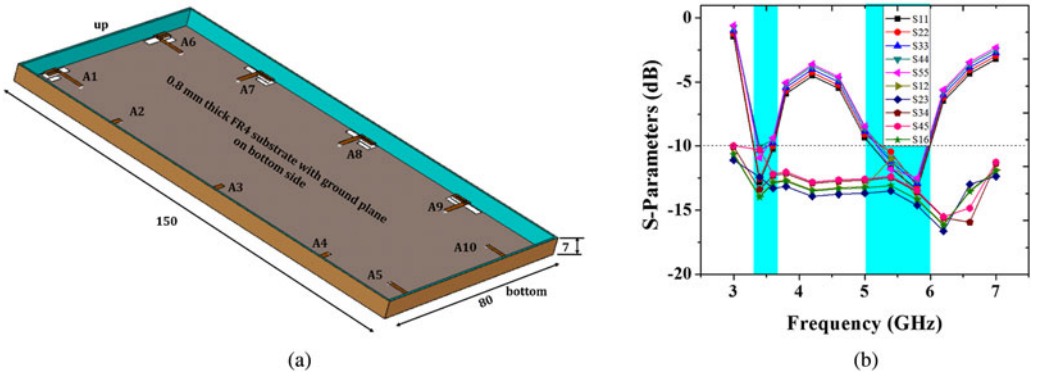

Fig. 22. (a) Proposed antenna with metal frame, (b) *S*-parameters.

Conclusion

A 10-port MIMO antenna system for 5G mobile phones operating at 3.4–3.6 and 5–6 GHz has been successfully investigated. The high isolation (>28 dB) among the adjacent antenna elements is achieved by placing the antenna elements orthogonally. Therefore, MIMO parameters such as ECC (<0.035) and TARC (>10 dB) are achieved better than their margin levels. The measured efficiency and gain of the proposed antenna range from 63 to 85% and 3 to 3.8 dBi, respectively. The calculated peak channel capacity in the 10 × 10 MIMO arrangement is achieved up to 48.5 bps/Hz for the low band and 51.7 bps/Hz for the higher band at 20 dB SNR. The proposed antenna has also shown better performance with the user's hand and SAR. Therefore, the 10-port antenna reported in this work could be a promising candidate for future mobile applications.

Acknowledgements. The authors wish to thank RF Centre of Excellence SASTRA-Keysight at SASTRA for their technical support in fabrication and measuring the antenna parameters

References

1. **Xu S, Zhang M, Wen H, Wen H and Wang J** (2017) Deep-subwavelength decoupling for MIMO antennas in mobile handsets with singular medium. *Scientific Reports* **7**, 12162, 1–9.
2. **Zhao A and Zhouyou R** (2019) Size reduction of self-isolated MIMO antenna system for 5G mobile phone applications. *IEEE Antennas Wireless Propagation Letters* **18**, 152–156.
3. **Sun L, Feng H, Li Y and Zhang Z** (2018) Compact 5G MIMO mobile phone antennas with tightly arranged orthogonal-mode pairs. *IEEE Transactions on Antenna and Propagation* **66**, 6364–6369.
4. **Li M-Y** (2017) Eight-port orthogonally dual polarised MIMO antennas using loop structures for 5G smartphone. *IET Microwaves and Antennas Propagation* **11**, 1810–1816.
5. **Parchin NO, Al-Yasir YIA, Ali AH, Elfergani I, Noras JM, Rodriguez J and Abd-Alhameed RA** (2019) Eight-element dual polarized MIMO slot antenna system for 5G smartphone applications. *IEEE Access* **9**, 15612–15622.
6. **Li M-Y, Ban Y-L and Xu Z-Q** (2018) Tri-polarized 12-antenna MIMO array for future 5G smartphone applications. *IEEE Access* **6**, 6160–6170.
7. **Abdullah M, Ban Y-L, Kang K, Li M-Y and Amin M** (2017) Eight-element antenna array at 3.5 GHz for MIMO wireless application. *Progress in Electromagnetic Research C* **78**, 209–217.
8. **Zhao X, Yeo SP and Ong LC** (2018) Decoupling of inverted-F antennas with high order modes of ground plane for 5G mobile MIMO platform. *IEEE Transactions on Antenna and Propagation* **66**, 4485–4495.
9. **Wong K-L, Lu J-Y, Chen L-Y, Li W-Y and Ban Y-L** (2016) 8-Antenna and 16-antenna arrays using the quad-antenna linear array as a building block for the 3.5-GHz LTE MIMO operation in the smartphone. *Microwave and Optical Technology Letters* **58**, 174–181.
10. **Parchin NO, Al-Yasir YIA, Noras JM and Abd-Alhameed RA** (2019) Dual-polarized MIMO antenna array design using miniaturized self-complementary structures for 5G smartphone applications. 13th European Conference on Antennas and Propagation (EuCAP 2019), Krakow, Poland, 31 March-5 April 2019, pp. 1–4.
11. **Li M-Y, Ban Y-L, Xu Z-Q, Wu G, Sim C-Y-D, Kang K and Yu Z-F** (2016) Eight-port orthogonally dual polarized antenna array for 5G smartphone applications. *IEEE Transactions on Antennas and Propagation* **64**, 3820–3830.
12. **Wong KL, Lu JY, Chen LY, Li W-Y, Ban Y-L and Li C** (2015) 16-antenna array in the smartphone for the 3.5-GHz MIMO operation. Asia Pacific Microwave Conference, pp. 1–3. doi:10.1109/APMC.2015.7411764
13. **Lu JY, Wong KL and Li WY** (2016) Compact eight-antenna array in the smartphone for the 3.5-GHz LTE 8×8 MIMO operation. Proceedings of IEEE 5th Asia-Pacific Conference on Antennas and Propagation, pp. 323–324. doi:10.1109/APCAP.2016.7843224
14. **Ban YL, Li C, Sim CYD, Wu G and Wong K-L** (2016) 4G/5G Multiple antennas for future multi-mode smartphone applications. *IEEE Access* **4**, 2981–2988.
15. **Zou H, Li Y, Sim C-Y-D and Yang G** (2018) Design of 8×8 dual band MIMO antenna array for 5G smartphone applications. *International Journal of RF and Microwave Computer-Aided Engineering* **28**, e21420.
16. **Li Y, Sim C-Y-D, Luo Y and Yang G** (2018) Multiband 10-antenna array for sub-6GHz MIMO applications in 5-G smartphones. *IEEE Access* **6**, 28041–28053. doi: 10.1109/ACCESS.2018.2838337.
17. **Dong J, Wang S and Mo J** (2020) Design of a twelve-port MIMO antenna system for multi-mode 4G/5G smartphone applications based on characteristic mode analysis. *IEEE Access* **8**, 90751–90759.
18. **Kumar N and Khanna R** (2020) A compact multi-band multi-input multi-output antenna for 4G/5 G and IoT devices using theory of characteristic modes. *International Journal of RF and Microwave Computer-Aided Engineering* **30**, e22012.
19. **Cui L, Guo J, Liu Y and Sim C-Y-D** (2019) An 8-element dual-band MIMO antenna with decoupling stub for 5 G smartphone applications. *IEEE Antennas and Wireless Propagation Letters* **18**, 2095–2099.
20. **Roy S, Biswas AK, Biswas S, Charraborthy U and Sarkhel A** (2021) Isolation improvement of dual-/quad-element textile MIMO antenna for 5G application. *Journal of Electromagnetic Waves and Applications*, 1–17. doi: 10.1080/09205071.2021.1888808.
21. **Li H, Sun S, Wang B and Wu F** (2018) Design of compact single-layer textile MIMO antenna for wearable applications. *IEEE Transactions on Antennas and Propagation* **66**, 3136–3141.
22. **Kumar Biswas A, Pattanayak SS and Chakraborty U** (2020) Evaluation of dielectric properties of colored resin plastic button to design a small MIMO antenna. *IEEE Transactions on Instrumentation and Measurement* **69**, 9170–9177.
23. **Guo J, Cui L, Li C and Sun B** (2018) Side-edge frame printed eight-port dual-band antenna array for 5G smartphone applications. *IEEE Transactions on Antenna and Propagation* **66**, 7412–7417.

https://doi.org/10.1017/S1759078721001112 Published online by Cambridge University Press

24. **Jiang W, Liu B, Cui YQ and Hu W** (2019) High-isolation eight element MIMO array for 5G smartphone applications. *IEEE Access* **7**, 34104–34112.
25. **Jiang W, Cui YQ, Liu B, Hu W and Xi Y** (2019) A dual-band MIMO antenna with enhanced isolation for 5G smartphone applications. *IEEE Access* **7**, 112554–112563.
26. **Xu H, Zhou H, Gao S, Wang H and Cheng Y** (2017) Multimode de coupling technique with independent tuning characteristic for mobile terminals. *IEEE Transactions on Antennas and Propagation* **65**, 6739–6751.
27. **Li MY, Ban YL, Xu ZQ, Wu G, Sim CYD, Kang K and Yu ZF** (2016) Eight-port orthogonally dual-polarized antenna array for 5G smartphone applications. *IEEE Transactions on Antenna and Propagation* **64**, 3820–3830.
28. **Li MY, Xu ZQ, Ban YL, Sim CYD and Yu ZF** (2017) Eight-port orthogonally dual-polarized MIMO antennas using loop structures for 5G smartphone. *IET Microwaves & Antennas Propagation* **11**, 1810–1816.
29. **Li YX, Sim CYD, Luo Y and Yang G** (2018) Multiband 10-antenna array for sub-6GHz MIMO applications in 5-G smartphone. *IEEE Access* **6**, 28041–28053.
30. **Liu Y, Ren AD, Liu H, *et al.***Wang and C. Sim, . (2019) Eight-port MIMO array using characteristic mode theory for 5G smartphone applications. *IEEE Access* **7**, 45679–45692.
31. **Sun LB, Feng HG and Li Y** (2018) Tightly arranged orthogonal mode antenna for 5G MIMO mobile terminal. *Microwave and Optical Technology Letters* **60**, 1751–1756.
32. **Sun LB, Feng HG, Li Y and Zhang Z** (2018) Compact 5G MIMO mobile phone antennas with tightly arranged orthogonal mode pairs. *IEEE Transactions on Antenna and Propagation* **66**, 6364–6369.
33. **Ren AD, Liu Y and Sim CYD** (2019) A compact building block with two shared-aperture antennas for eight-antenna MIMO array in metal-rimmed smartphone. *IEEE Transactions on Antenna and Propagation* **67**, 6430–6438.
34. **Wong KL, Tsai CY and Lu JY** (2017) Two asymmetrically mirrored gap-coupled loop antennas as a compact building block for eight-antenna MIMO array in the future smartphone. *IEEE Transactions on Antenna and Propagation* **65**, 1765–1778.
35. **Wong KL, Chen YH and Li WY** (2018) Decoupled compact ultra-wideband MIMO antennas covering 3300–6000 MHz for the fifth-generation mobile and 5 GHz WLAN operations in the future smartphone. *Microwave and Optical Technology Letters* **60**, 2345–2351.
36. **Wong KL, Lin BW and Lin SE** (2019) High-isolation conjoined loop multi-input multi-output antennas for the fifth-generation tablet device. *Microwave and Optical Technology Letters* **61**, 111–119.
37. **Tsai CY, Wong KL and Li WY** (2018) Experimental results of the multi-GBPs smartphone with 20 multi-input multi-output (MIMO) antennas in the 20×12 MIMO operation. *Microwave and Optical Technology Letters* **60**, 2001–2010.
38. **Zhang XG, Li YX, Wang W and Shen W** (2019) Ultra-wideband 8-port MIMO antenna array for 5G metal-frame smart phones. *IEEE Access* **7**, 72273–72282.
39. **Lu JY, Chang HJ and Wong KL**, 10-Antenna array in the smartphone for the 3.6-GHz MIMO operation. Proceedings of IEEE International Symposium on Antennas and Propagation & USNC/URSI National Radio Science Meeting, 2015, pp. 1220–1221. doi:10.1109/APS.2015.7304999
40. **Wong KL, Chang HJ and Li WY** (2018) Integrated triple wide band triple-inverted-F antenna covering 617–960/ 1710–2690/3300–4200 MHz for 4G/5G communications in the smart phone. *Microwave and Optical Technology Letters* **60**, 2091–2096.
41. **Huang C, Jiao YC and Weng ZB** (2018) Novel compact CRLHTL-based tri-band MIMO antenna element for the 5G mobile handsets. *Microwave and Optical Technology Letters* **60**, 2559–2564.
42. **Chen QG, Lin HW, Wang JP, Ge L, Li YJ, Pei TQ, Sim CYD and Ge L** (2019) Single ring slot-based antennas for metal-rimmed 4G/5G smartphones. *IEEE Transactions on Antenna and Propagation* **67**, 1476–1487.
43. **Deng CJ, Liu D and Lv X** (2019) Tightly-arranged four-element MIMO antennas for 5G mobile terminals. *IEEE Transactions on Antenna and Propagation* **7**, 6353–6361. doi: https://doi.org/10.1109/TAP.2019.2922757
44. **Li YX, Sim CYD, Luo Y and Yang G** (2019) High-isolation 3.5 GHz eight-antenna MIMO array using balanced open-slot antenna element for 5G smart phones. *IEEE Transactions on Antenna and Propagation* **67**, 3820–3830.
45. **Wang C, Xiao S, Wang W, Wang C and Liu S** An analytical approach for antenna performance evaluation for MIMO systems. 2015 International Symposium on Antennas and Propagation (ISAP), 2015, pp. 1–4.
46. **Balanis CA** (2005) *Antenna Theory Analysis and Design*. United States: John Wiley & Sons.

D. Rajesh Kumar was born in Madurai, Tamilnadu, India in 1987. He obtained B.E. in electronics and communication engineering from Anna University, Tamilnadu, India in 2008 and M.E. in communication systems from Anna University, Tamilnadu, India in 2013. He has 9 years of teaching experience as assistant professor in SACSMAVMM Engineering College, Madurai, India. Currently, he is working as a research assistant and pursuing Ph.D. in the field of antennas for 5G communications in SASTRA Deemed University, Tamilnadu, India. His research areas include mobile phone antenna design and RF system design.

G. Venkat Babu is assistant professor in the Department of Electronics and Communication, SEEE, SASTRA Deemed University, Tamilnadu, India. He obtained B.E. in electronics and communication from Bharathidasan University, Trichy, M.E. in microwave communication and radar from Dr. B.R. Ambedkar University, Agra, India and Ph.D. in electronics and communication from Bhagwant University, Ajmer, India. His research is related to reconfigurable antenna and RF-MEMS. He has academic and research experience of about 19 years. He has published his research work in reputed journals, international and national conferences. He co-authored a book in the area of electromagnetic fields. He is a member of IEEE (Society APS & MTS), life member. of IETE and ISTE.

K.G. Sujanth Narayan was born in Chennai, Tamilnadu, India, in 1996. He obtained B.E. in electronics and communication engineering from R.M.K. Engineering College, Kavarapettai, Tamilnadu and M.Tech. in communication systems from SASTRA Deemed University, Thanjavur, Tamilnadu in the years 2017 and 2019, respectively. Currently, he is working as a research assistant and pursuing Ph.D. in the area of antennas and RF system design from School of Electrical and Electronics Engineering, SASTRA Deemed University, Thanjavur, Tamilnadu. He is a member of IEEE. His research areas include antennas, electromagnetics, RF system design, EMI/EMC and vehicular communication.

N. Raju obtained M.E. in applied electronics from Anna University, and Ph.D. in speech processing from SASTRA Deemed to be University, India. His main research interests are robotics, embedded systems, VLSI design, speech processing, and machine learning. He has published more than 30 research papers in reputed international journals and conferences. He is currently working as senior assistant professor in the Department of ECE, School of EEE, SASTRA Deemed University, Thanjavur. He is a life member of the Indian Society of Systems for Science and Engineering (ISSE).

https://doi.org/10.1017/S1759078721001112 Published online by Cambridge University Press